Main Manuscript for

Reduced global fire activity due to human demography slows global warming by enhanced land carbon uptake

Chao Wu[a,b,c*], Stephen Sitch[b], Chris Huntingford[d], Lina M. Mercado[b,d], Sergey Venevsky[a,e], Gitta Lasslop[f], Sally Archibald[g], A. Carla Staver[c,h]

[a] Ministry of Education Key Laboratory for Earth System Modeling, Department of Earth System Science, Tsinghua University, Beijing 100084, China; [b] College of Life and Environmental Sciences, University of Exeter, Exeter EX4 4QF, UK; [c] Department of Ecology and Evolutionary Biology, Yale University, New Haven, CT 06511, USA; [d] UK Centre for Ecology and Hydrology, Wallingford, Oxfordshire OX10 8BB, UK; [e] The Southern Scientific Centre of The Russian Academy of Sciences, Rostov-on-Don, 344006, Russian Federation; [f] Senckenberg Biodiversity and Climate Research Centre, Frankfurt am Main, Hesse 60345, Germany; [g] Centre for African Ecology, School of Animal, Plant and Environmental Sciences, University of the Witwatersrand, Johannesburg 2050, South Africa; [h] Yale Institute for Biospheric Studies, Yale University, New Haven, CT 06511, USA.

***** Chao Wu, Department of Ecology and Evolutionary Biology, Yale University, New Haven, CT 06511, USA

Email: chaowu.thu@gmail.com; phone number: (+1) 2032850043

Classification

BIOLOGICAL SCIENCES: Ecology

PHYSICAL SCIENCES: Earth, Atmospheric, and Planetary Sciences

Keywords

Fire; climate-carbon cycle feedback; carbon sink; dynamic global vegetation model (DGVM); climate change; human demography.

Author Contributions

S.S., C.W., C.H., L.M.M., and S.V. designed research; C.W. performed the simulations; C.W., S.S., C.H., L.M.M., S.V., G.L., and A.C.S. performed the analysis; C.W. wrote the first draft with input from C.H., S.S., L.M.M., A.C.S., G.L., S.V., and S.A., and all authors contributed to the interpretation of the results and writing of the paper.

This PDF file includes:

Main Text

Figures legends

Abstract

Fire is an important climate-driven disturbance in terrestrial ecosystems, also modulated by human ignitions or fire suppression. Changes in fire emissions can feed back on the global carbon cycle, but whether the trajectories of changing fire activity will exacerbate or attenuate climate change is poorly understood. Here, we quantify fire dynamics under historical and future climate and human demography using a coupled global climate-fire-carbon cycle model that emulates 34 individual Earth System Models (ESMs). Results are compared to counterfactual worlds, one with a constant preindustrial fire regime and another without fire. Although uncertainty in projected fire effects is large and depends on ESM, socioeconomic trajectory, and emissions scenario, we find that changes in human demography tend to suppress global fire activity, keeping more carbon within terrestrial ecosystems and attenuating warming. Globally, changes in fire have acted to warm climate throughout most of the 20th century. However, recent and predicted future reductions in fire activity may reverse this, enhancing land carbon uptake, and corresponding to offsetting ~5-10 years of global CO_2 emissions at today's levels. This potentially reduces warming by up to 0.11°C by 2100. We show that climate-carbon cycle feedbacks, as caused by changing fire regimes, are most effective at slowing global warming under lower emission scenarios. Our study highlights that ignitions and active and passive fire suppression can be as important in driving future fire regimes as changes in climate, although with some risk of more extreme fires regionally and with implications for other ecosystem functions in fire-dependent ecosystems.

Significance Statement

Fire is an increasing climate-driven threat to humans. While human demography can strongly modulate fire ignition rates or fire suppression, changes in CO_2 released by fires feed back to climate. We show that human demography could reduce future fire activity, which would in turn attenuate global warming via an enhanced land carbon sink. This mitigation is strongest in a low CO_2 emission world, corresponding in magnitude to ~5-10 years of global CO_2 emissions at today's levels by 2100. We highlight the strong role of human demography in global fire reduction, and the potential for climate change mitigation by enhanced land carbon sequestration. We also note possible trade-offs, including loss of biodiversity in fire-dependent ecosystems and increases in severe fire events.

Main Text

Introduction

Biomass burning is a significant component of the global carbon cycle, releasing around 2.2 Pg C yr^{-1} to the atmosphere(1). Some of this carbon is taken up again as biomass regrows, but fire exclusion experiments(2) and model simulations(3-5) show that fire has decreased ecosystem carbon storage in the past. As fire regimes are changing globally, we should expect changes of sufficient magnitude to affect the global carbon cycle and to feed back to climate(6). The trajectories and outcomes of these changes are uncertain, however. On the one hand, a positive feedback may occur, whereby climate change causes more fires, releasing extra CO_2 and intensifying warming(7). This possibility is consistent with sedimentary charcoal records showing that biomass burning increases with temperature(8), and with model projections suggesting that climate change will increase fire activity(9). On the other hand, human intervention in the recent past may have instead reduced historical global fires and associated CO_2 emissions, enhancing global land carbon uptake(10), a mechanism that is usually overlooked in terrestrial carbon assessments(11) or in climate projections using standard biomass burning emission datasets used to force Earth System Models (ESMs). An increased land carbon sink acts as a negative feedback and may attenuate global warming(12, 13). These two opposing mechanisms are probably both operating but may exhibit substantial regional differences and may also change as climate and human demographics change. Their additive and interactive effects for the Earth system are uncertain, however, and a deeper understanding of historical fire dynamics will improve future projections of fire activity and capture the transient net fire effects on the land carbon balance and, critically, any potential to reinforce or mitigate climatic changes.

The dynamics of fire events are controlled by a variety of climatic and human factors (*e.g.*, demography, land-use, and socioeconomics). Climate influences fire activity in part by affecting plant growth and competition, thus resulting in changes in vegetation composition and associated flammability(14). Climate may also alter drought conditions, affecting fuel aridity and thus fire characteristics(15). Direct human impacts are highly important, as population density determines anthropogenic ignitions(16, 17). Indirect effects such as cropland expansion and landscape fragmentation decrease burned area in flammable ecosystems, including savannas(10, 18, 19). Meanwhile, urbanization can increase burned area by growing the Wildland-Urban Interface (WUI)(20) and potentially increasing human ignitions(21). Yet urbanization (*e.g.*, urban expansion), by bringing human settlements into closer proximity to potential wildfires, can instead result in active and passive fire suppression to reduce risks to health and safety(22). With increasing pressure on natural systems from humans, global-scale studies suggest that these human factors are among the dominant controls on fire dynamics in many ecosystems(14, 18, 23).

Because the response of fire to changes in climate and human factors are complex(14, 18), predicting long-term trajectories of future fire emissions is challenging(24), resulting in large uncertainties in the estimate of feedbacks between terrestrial ecosystems, fire, and climate(25). In an Earth system context, studies have investigated the effects of fire on climate-carbon cycle feedbacks using only highly simplified box models of the land biosphere(7) and/or utilizing only single Earth System Models (ESMs)(4, 26). This limits our quantitative understanding of the robustness of potential future effects of fire in either speeding or slowing global warming. To address these issues, we combined a global fire model that can reproduce the recent human-driven fire dynamics with a Dynamic Global Vegetation Model (DGVM), then coupled it within an Earth system emulator which integrates 34 ESMs, using various scenarios of CO_2 emissions and demographic developments, to quantify CO_2 feedbacks between terrestrial ecosystems, fire, and climate. This approach considers the effects of humans, vegetation, and climate on fire and allows us to estimate the uncertainties related to climate projections and demographic developments.

We first evaluated the performance of the fire-enabled DGVM (LPJ-SEVER; see Materials and Methods) when forced with observed historical climatology. Our DGVM estimates of the recent past are tested against datasets of satellite-based burned area, fire emissions products, and land biogeochemistry. We next forced the coupled climate-fire-carbon cycle model with climate change patterns from 34 ESMs, to investigate the long-term fire dynamics for the period 1860-2100 inclusive. Emulating multiple ESMs enabled the capture of uncertainty in climate change. Each simulation was then driven with observed historical and projected future emissions from the four Representative Concentration Pathways (RCPs)(27) (*i.e.*, 34 ESMs × 4 RCPs simulations). Each RCP was initially aligned with a demographic scenario that described different population growth and urbanization rates, based on combined features from the established Shared Socioeconomic Pathways (SSPs)(28) (see Table 1 and Materials and Methods). In total we had 136 'standard' simulations (34 ESMs × 4 RCPs), which together comprised 'climatic uncertainty'. We also performed a second set of 'constant fire' simulations with a constant preindustrial fire regime; for each grid cell, we generated a fixed 241-year time series of burned area using preindustrial climate and its variability, which we then used to force the dynamic model during the transient period to year 2100, with all else being the same as the 'standard' simulations. The difference between the 'standard' and 'constant fire' simulations was used to quantify the climate-carbon cycle feedbacks derived from changing fire frequencies. Finally, we further performed a third set of identical simulations to 'standard' experiment, except with the fire model switched off (*i.e.*, 'without fire' simulations). The difference between the 'standard' and 'without fire' simulations determines the net overall contributions of fire to changes in the land carbon balance and any resultant climatic feedbacks by modulating time-evolving atmospheric CO_2 levels (Materials and Methods).

To further characterise the uncertainties related purely to the human influence on fire dynamics, we performed an additional set of simulations using four RCP scenarios and 9 SSP combinations (36 combinations) that covered the full range of possible population growth and urbanization rates within our three SSPs, and for each RCP. These extra simulations represent 'demographic uncertainty' (SI Appendix, Table S1), and for each, an identical 'constant fire' simulation and 'without fire' simulation were also performed. In this assessment of uncertainty in SSP combinations, one ESM with mid-range future warming was used (CESM1-BGC; SI Appendix, Table S2).

Results

Model evaluation

The model estimated a negative global burned area trend, with a rate of -2.62 Mha yr^{-2}, which fell in the observational bounds from satellite-based estimates of -1.89 to -5.31 Mha yr^{-2}. Simulated mean annual burned area (423.16 Mha yr^{-1}) fell within the observed range from FireCCI50 (387.39 Mha yr^{-1}), GFED4 (346.42 Mha yr^{-1}) and GFED4s (486.07 Mha yr^{-1}) datasets, as averaged over the period 1997-2013 (Fig. 1A). The simulated mean annual fire carbon emission was 2.33 Pg C yr^{-1}, similar to 2.18 Pg C yr^{-1} from the widely used GFED4s dataset, but lower than a Fire Radiative Power (FRP)-based FEER1 dataset (3.73 Pg C yr^{-1}) (Fig. 1B). Our results in simulating historical fire were also within the range of the Fire Modeling Intercomparison Project (FireMIP) models ([354 - 531 Mha yr^{-1}] for burned area(29) and [1.0 - 4.9 Pg C yr^{-1}] for fire carbon emissions(30)). When considered geographically, the simulated and observed patterns of mean annual fire carbon emissions and burned area agreed well in most regions (SI Appendix, Figs. S1 and S2). Across different biomes, we broadly reproduced fire carbon emissions and burned area in temperate and boreal forests; however, comparing to GFED4s and FEER1datasets, respectively, we underestimated by 69% and 81% fire carbon emissions in tropical forests (associated with ground fires associated with degradation, and deforestation fires) and overestimated by 126% and 0% those in grasslands (SI Appendix, Tables S3 and S4), although we also note that recent satellite products that include a small-fire correction suggest much higher area burnt and emissions(31). Further evaluation i) of simulated grid-cell based temporal burned area and fire carbon emissions (SI Appendix, Fig. S3) and ii) of carbon and water cycling using the International Land Model Benchmarking (ILAMB) system (SI Appendix, Fig. S4 and Tables S2 and S5) demonstrated a satisfactory DGVM and fire module performance at reproducing historical fire regime and terrestrial ecosystem carbon fluxes and pools. An assessment of the simulated present-day global vegetation distribution is shown in SI Appendix, Fig. S5.

Fig. 1

Long-term fire dynamics and impact on land carbon balance

The 'standard' simulations showed reductions in global fire carbon emissions from the 1950s relative to 'constant fire' simulations, due largely to human demographic changes(14, 32) (SI Appendix, Figs. S6 and S7), likely attributable to fire suppression(10, 33, 34), landscape fragmentation(10, 18), and agricultural expansion(18, 35). Future reductions in fire carbon emissions diverged depending on RCP (Fig. 2A and Table 1). Notably, the spread of uncertainty within each RCP was substantially larger across different demographic scenarios than it was across different ESMs (Fig. 2A vs. B). However, across RCPs, climatic uncertainty was larger than demographic uncertainty, with mean annual reductions in fire emissions during 2081-2100 relative to 'constant fire' simulations ranging from -1.69 ± 0.19 to -2.62 ± 0.23 Pg C yr^{-1} and -2.18 ± 0.47 to -2.25 ± 0.54 Pg C yr^{-1}, respectively (Fig. 2A; means of 34 ESMs, uncertainty bounds are $\pm$ 1 standard deviation; Fig. 2B; means of 9 SSP combinations).

These results demonstrated that, irrespective of ESM emulated, RCP, or demographic scenario, simulated fire carbon emissions are predicted to remain lower than preindustrial levels. In addition, many simulations showed further reductions in fire carbon emissions compared to present day (year 2020). Notably, under the 'climatic uncertainty' simulations (Fig. 2A), future fire carbon emissions were larger under RCP2.6 than under RCP4.5 and 6.0 (SI Appendix, Fig. S8), largely because future population growth was faster in RCP2.6 than RCP4.5 (Table 1; see also ref. (36)), resulting in more human ignitions but accompanied by slower urbanization (*e.g.*, reduced urban expansion) in RCP2.6 than RCP6.0 (Table 1), resulting in less fire suppression, longer fire duration, and thus larger fire emissions (SI Appendix, Fig. S7). Notably, future fire emissions were highest under RCP8.5 (SI Appendix, Fig. S8), which demonstrates that, although fires are sensitive to demographic futures, climate change will also have a substantial impact on future fire frequency, especially when climate change is severe.

We also found that the reduction of global fire carbon emissions from the 1950s has contributed to an enhanced land carbon sink (Fig. 2C, D; see also refs. (10, 11)). These trends also continued into the future in most modelled scenarios. Curiously, enhanced land carbon uptake from reductions in fire activity was larger in the future (*i.e.*, RCP2.6 and 8.5 scenarios) than it was over the historical period (global mean annual Net Biome Production [NBP] = 0.40 ± 0.04 and 0.59 ± 0.27 Pg C yr^{-1} for future [2081-2100] in RCP2.6 and RCP8.5, respectively vs. 0.18 ± 0.03 Pg C yr^{-1} over the historical period [1986-2005]; Fig. 2C, SI Appendix, Fig. S9). Consistent with ref. (11), the global NBP difference between the simulations with changing fire and with constant fire is associated both with the indirect effects of fire and its change through time on component fluxes, Gross Primary Productivity (GPP) and Terrestrial Ecosystem Respiration (TER), and from reductions in fire carbon emissions themselves (FC) (NBP=GPP-TER-FC; see Materials and Methods; SI Appendix, Fig. S9). Future NBP changes varied regionally (Fig. 2E, F and SI Appendix, Figs. S10 and S11), with the largest enhancements in land carbon uptake expected in regions most frequently disturbed by fires(11), including the Brazilian *cerrado*, mesic African savannas, Southeast Asia, and the northern Eurasia (Fig. 2E, F).

Table 1

Fig. 2

Climate-carbon cycle feedbacks derived from changing fires

As noted, in all climate and demographic scenarios, reductions in simulated future fire carbon emissions mean that they remained below preindustrial levels (Fig. 2A, B). When compared to simulations with 'constant fire', this led to an enhanced land carbon sink by 2100 (Fig. 2C, D). The simulation with changing and with constant fire started with an NBP of zero at equilibrium in 1860. Increases in atmospheric CO_2 and climate change affected productivity over time in both simulations. As fire reduced biomass storage, a reduction in fire frequency over time in the simulation with changing fire led to an increase in biomass build-up, additionally facilitated by shifts from grasses to trees (*i.e.*, woody encroachment which constitutes a major threat to fire-dependent ecosystems; SI Appendix, Fig. S12). As both simulations started with the same atmospheric CO_2 concentration, reductions in fire frequency, and enhanced land carbon sink, corresponded to a relative decline in atmospheric CO_2 (Fig. 3A, B), and thus to attenuated warming (Fig. 3C, D). We found a reversal of the fire-climate-carbon cycle feedback (*i.e.*, fire-induced changes in land carbon balance and further feedback to climate) in the future, leading to a net cooling effect from slight warming throughout most of the 20th century (1860-1978; Fig. 3C). Under the RCP2.6 scenarios, reductions in fires lowered the global mean annual temperature relative to 'constant fire' simulations by 0.06 ± 0.01 °C and 0.08 ± 0.02 °C for the period 2081-2100, across the range of ESMs and demographic scenarios, respectively (Fig. 3C, D, right-hand marked uncertainty bounds). Corresponding values for RCP8.5 were similar, *i.e.*, 0.07 ± 0.01 °C and 0.06 ± 0.01 °C. Notably, the strongest cooling was obtained with RCP4.5 (0.09 ± 0.01 °C) and RCP2.6 (0.08 ± 0.02 °C) taking into account the 'climatic uncertainty' and 'demographic uncertainty' (Fig. 3C, D), and for these cases where fire emissions were projected to continuously decrease in the future (SI Appendix, Fig. S8). In sum, human demographic changes have resulted in fire suppression globally, reducing fire activity – for instance through urbanization (*i.e.*, urban expansion & increasing WUI) and changing agricultural land use. This, in turn, has enhanced net land carbon uptake and is likely to continue to do so, resulting in a net negative feedback on global warming.

Our simulations revealed multiple key interactions between the climate-carbon cycle system and fire effects. First, the order and relative magnitudes of the reductions in fire carbon emissions curves (Fig. 2A, B) differed from those for enhanced land carbon uptake (Fig. 2C, D). Crucially, although fire effects on atmospheric CO_2 concentrations were smaller in RCP2.6 and RCP4.5 than in RCP8.5 (Fig. 3A, B), simulations under RCP2.6 and RCP4.5 had a larger cooling effect (Fig. 3C, D; this pattern is clearer in 'demographic uncertainty' simulations). This reversal is due to the logarithmic relationship between changes in CO_2 and radiative forcing, which is a metric of thermal response to changing atmospheric greenhouse gas concentrations. Hence, a unit of CO_2 suppressed at low concentration levels (*e.g.*, under RCP2.6 and RCP4.5) will have a stronger cooling effect. The higher temperature-CO_2 sensitivity at lower CO_2 emission scenarios (Fig. 3E, F) implies greater relative importance of reductions in fire emissions under low fossil-fuel RCP scenarios, which has direct relevance to global policies for constraining global warming.

Fig. 3

Influence of demographic changes on projected global temperature

To further understand demographic effects on fire carbon emissions and climate at a global scale, simulations based on every possible combination of population growth and urbanization rate were performed (Fig. 4 and SI Appendix, Table S1). These additional analyses were performed only for the RCP2.6 scenario. Results showed that a rapid increase in population (*i.e.*, more human ignitions) combined with slow urbanization (*i.e.*, longer distance from cities, less fire suppression and longer fire duration) led to the highest fire emissions and least cooling, while slow population growth and rapid urbanization led to the lowest emissions and most cooling (Fig. 4A, B). Uncertainty associated with population density and urbanization translated to a large uncertainty in the cooling effect of fewer fires (0.05 – 0.11 °C) in 2100. These results highlight the roles of population increase and urbanization for simulating fire activity trends in the future.

Fig. 4

A net overall negative effect of future fire on global climate: results from a world without fire

In addition to using a counterfactual 'constant fire' experiments, simulations with a world without fire have been used to capture the effect of fire on global carbon cycle and ecosystem composition by DGVMs(3, 5, 37, 38). These capture the net contributions of fire to the land carbon balance and any resultant climatic feedbacks by comparing the difference in global temperature between 'standard' and 'without fire' simulations. Overall, these simulations also support the conclusion that future decreases in fire activity globally have a consistent relative cooling effect on global temperature but suggest a smaller magnitude temperature reduction than comparison with constant fire simulations suggest. These result from a smaller enhanced land carbon uptake in all RCP scenarios (Fig. 5A, B and SI Appendix, Figs. S13C, D and S14A-D). Nevertheless, the spatial patterns of the fire-induced enhanced land carbon sink were highly consistent with those from the difference in NBP between 'standard' and 'constant fire' simulations (SI Appendix, Fig. S14E, F vs. Fig. 2E, F). Overall, under the RCP2.6 scenario, future fire lowered the global mean annual temperature relative to 'without fire' simulations by 0.03 ± 0.01 °C and 0.04 ± 0.02 °C for the period 2081-2100, across the range of ESMs and demographic scenarios, respectively (Fig. 5A, B and SI Appendix, Fig. S13C, D). Similarly, the strongest cooling was obtained under RCP4.5 (0.05 ± 0.02 °C) and RCP2.6 (0.04 ± 0.02 °C) considering the 'climatic uncertainty' and 'demographic uncertainty' during 2081-2100 (Fig. 5A, B and SI Appendix, Fig. S13C, D). Across different combinations of population growth rates and urbanization rates, again consistent with 'constant fire' experiments, slow population growth and rapid urbanization also led to the lowest emissions and most cooling. However, by year 2100 for the high climate mitigation RCP2.6 scenario, simulated fire trajectories reduced warming by 0.08 °C against the world 'without fire' (SI Appendix, Fig. S15B), compared to 0.11 °C against the 'constant fire' reference (Fig. 4B).

Fig. 5

Discussion and Conclusions

Here, we project that recent decreases in fire activity will continue into the next century, reducing future fire carbon emissions and attenuating global warming through enhanced land carbon uptake. These results contradict predictions that include only the effects of future fire weather(9, 39) and demonstrate that ignition, fire suppression, and fuel fragmentation impacts on fire need to be considered for accurate estimates of fire-induced climate-carbon cycle feedbacks. We show that terrestrial ecosystems sequestered an additional 10-21 ppm in CO_2 concentration from the atmosphere due to reduced fire emissions by 2100 under all scenarios compared to a world with a 'constant fire' regime (mean of 34 ESMs). This reduction in atmospheric CO_2 corresponds to between 173 and 363 Pg CO_2 of emissions into the atmosphere, equal to 5-10 years of global fossil fuels and industrial CO_2 emissions at today's levels(40). This calculation assumes that the global natural sinks (land and ocean) absorb approximately 55% of anthropogenic emissions, so the 'airborne fraction' added to the atmosphere is about 45%; today's (year 2019) fossil fuels and industrial CO_2 emissions is around 37 Pg CO_2 emission from ref.(40). Under scenarios where the world introduces major efforts to mitigate emissions, then the equivalent years of emissions saved could become substantially longer than the 5-10 years we estimate here, implying a strong potential of human actions to disturb the Earth system by changing fire frequencies.

The magnitude of this relative cooling effect will depend on indirect effects of an enhanced land carbon sink and on direct effects from reduced fire carbon emissions themselves. Here, the indirect effect (i.e., changes in ecosystem respiration and productivity) of fire decline on NBP was roughly similar in magnitude to the corresponding direct impacts on fire carbon emissions reductions (SI Appendix, Fig. S9), arising in part from changes in vegetation composition (*i.e.*, Plant Function Types [PFTs]; see Materials and Methods). That is to say, there is a trade-off between increases in land carbon storage and risks of the fire-dependent ecosystems losses (*e.g.*, tropical savannas and grasslands) through time via fire suppression (SI Appendix, Fig. S16). Our findings are also qualitatively in line with general analysis of forest disturbances under climate change, particularly regarding long-term trends and patterns, and effects of interaction and feedbacks(41). Indirect climate effects such as vegetation dynamics can dampen long-term sensitivity of disturbance to climate, despite the possibility of amplification of disturbances under climate change due to interaction of mainly abiotic influencing agents (drought, wind, snowpack, and ice), which is captured in our DGVM. Overall, results suggest that ongoing refinement of DGVMs to constrain their estimates of the dynamic balance of land carbon will be essential to predict the future land carbon sink strength and potential feedback to climates, particularly in interaction with fire.

In the real world, these changes in fire activity have large consequences for other elements of ecosystem function beyond carbon storage. For instance, declining fire activity and resulting woody encroachment often has negative effects on fire-dependent ecosystems(42), and in particular on tropical savannas and grasslands(43, 44), where fire is crucial for ecosystem function and maintenance of biodiversity(45, 46) and human livelihoods(47). This link has been demonstrated empirically: increases in carbon stocks resulting from fire suppression in savannas have been associated with extensive biodiversity losses(45). In other fire-dependent systems, including the Mediterranean and coniferous systems, overall decreases in burned area can also increase severe fire risk via increases in fuel loads. In these areas, fire management to mitigate the risk of catastrophic fire in existing and newly emerging fire-prone areas(14) may also be preferable to carbon storage from a policy standpoint.

Our analysis of demographic factors reveals that change in fire activity are determined by the interplay between increasing population density, which increases fire ignitions and area burned, and increasing urbanization (*e.g.*, urban expansion), which promotes active and passive fire suppression in the WUI. We here assumed that fire activity is a deterministic outcome of human demography, ignoring the leverage that real fire policy and management may have in determining fire activity(10), so results should not be interpreted to mean that fire suppression is an effective or desirable tool for carbon storage, especially given risks of extreme fires that are known to result from fire suppression(48). Given the importance of human decisions for shaping fire activity(49), additional investment in explicitly incorporating interactive fire management into global models may also be fruitful.

Our analysis also reveals an interesting scenario dependency. In low emissions scenarios, RCP2.6 and RCP4.5, the contributions of human-driven reduction in fire carbon emissions to the enhanced land carbon sink are smaller in magnitude compared to the high emissions RCP6.0 and RCP8.5 scenarios. However, despite lower uptake, there is greater relative cooling projected for RCP2.6 and RCP4.5, because the per-unit effect of increasing atmospheric CO_2 on warming is greater at lower CO_2 concentrations. Thus, reductions in fire carbon emissions due to human factors, *e.g.*, fire suppression(10, 33, 34), cropland expansion(18, 35), and deliberate increases in landscape fragmentation resulting from cultivation and livestock grazing(10, 18), will have a larger impact on global climate if society takes concrete action towards commitments to constraining warming to 2 °C, or even 1.5 °C, since the preindustrial period(50).

Here, we constrain our attention to changing fire-related emissions of CO_2, and its impact on global temperature. This focus on the global carbon cycle ignores biophysical feedbacks, which can have major impacts on near-surface climate via effects on albedo(51) and heat and moisture fluxes(52) and which also include atmospheric feedbacks via aerosol forcing(4, 51, 53). However, these biophysical effects of fire on climate remain largely uncertain(25) at both global(54) and regional scale(51, 54, 55), and must be better quantified before they can be meaningfully integrated into assessments of fire interactions with climate change. Although our spread of simulations captures many of the uncertainties in the estimate of fires from climate and human demography, caution should also be exercised as our results are from a single DGVM and with a single fire module. Intercomparison studies are needed; these could use our simulation structure, which captures the uncertainties intrinsic to climate predictions and demographic scenarios but should further include multiple DGVMs and fire components to more fully represent the uncertainties associated with fire as a process. Accurate regional-scale fire activity trajectories are becoming increasingly necessary in the context of changing climate, fire regimes and socioeconomic forcings. To achieve this, we need a range of models that more fully represent different mechanistic schemes for fire. SEVER-FIRE captures fire suppression trends that characterize fire regimes in recent decades, but regional studies show that fire activity is increasing even with active fire suppression measures in place(56, 57). SEVER-FIRE assumes that future fire suppression will be mainly focused on the protection of valuable infrastructure and human life and thus will be concentrated mainly around WUI. However, SEVER-FIRE does not yet account for fire suppression–fire weather relationship linkages found recently for Southern Europe(56), which predict that fire suppression can change the response of burned area to weather, increasing burned area by 30% by the end of this century despite fire suppression under a high emission scenario. These changes in fire danger following active fire suppression are only crudely represented in global fire models in DGVMs but should be a priority for future research.

In conclusion, we illustrate that human demographic change is likely to reduce future global fire activity and that this decreasing trend could reduce direct fire carbon emissions and indirectly enhance land carbon uptake. Together, these generate a relative cooling effect that attenuates ongoing global warming. Although the fire model captures recent human-driven fire dynamics, human demographic effects on fire regimes are not currently well-constrained, which creates considerable uncertainties in projected fire dynamics. For any particular RCP scenario, the size of uncertainty in this relative cooling effect due to different demographic scenario is of similar magnitude to that caused by differences in predictions by alternative ESMs. We show that the impact of climate-carbon cycle feedbacks derived from changing fires are strongest at slowing global warming under the lower emission scenarios (RCP2.6 and 4.5). In addition to the benefit of increased carbon storage, decisions to safeguard future human well-being need to consider the negative side-effects of fire suppression, including biodiversity loss in fire-dependent ecosystems and increased risk of dangerous and severe fire events. Finally, it is crucial to note that any gains in carbon storage from decreased fire activity should not be considered a substitute for other climate action. Nature-based solutions, including fire management, cannot substitute for emissions reductions for constraining global warming to existing targets (*e.g.*, 1.5 or 2 °C above preindustrial levels).

Materials and Methods

LPJ-SEVER model

Our process-based fire model is SEVER-FIRE (Socio-Economic and natural Vegetation ExpeRimental global FIRE model)(33). This model framework simulates fire dynamics and the role of fire in the Earth system, and here is coupled to the Lund-Potsdam-Jena Dynamic Global Vegetation Model (LPJ-DGVM), which includes 10 Plant Function Types (PFTs)(58). Human-and lightning-ignited fires are separately represented in SEVER-FIRE. This simulation system (LPJ-SEVER) accounts for population density and urbanization (urban expansion & increasing WUI) as two main demographic factors in regulating human-ignited fires (SI Appendix, Fig. S7). Lightning-ignited fires are regulated by convective precipitation which is a climatic proxy of number of cloud-ground lightning strokes(33). Fire carbon emissions are calculated based on ref. (59), where we assumed two-thirds of woody biomass is above-ground and applied a Combustion Completeness (CC) to represent the fraction of available fuel load will be burned during a fire. The biomass consumed by fire goes directly into the atmosphere (immediate, direct fire emissions). Remaining burned biomass becomes litter which will further decompose during post-fire years (legacy fire emissions). Here, we apply a separate global GFED-based averaged CC for biomass (0.427) and litter (0.847)(60) in SEVER-FIRE. Note, in our experimental design (with changing fire versus with constant fire/without fire) we thus implicitly account for i) direct emissions (*i.e.*, annual fire carbon flux) ii) legacy carbon fluxes associated with fire-related mortality, and iii) loss/additional carbon sink capacity with more Leaf Area Index (LAI) and differential response to climate change with changing fire and with constant fire/without fire. Therefore, by inclusion of the two additional processes (mortality and LAI effects), the true fire carbon emissions are larger than those based on direct annual carbon emissions alone(61). Thus, a DGVM is an ideal tool to study tropical forest degradation through fire, where direct emissions represent a smaller fraction than legacy emissions associated with tree mortality, necromass decomposition, and forest regrowth/recovery(62).

A unique feature of SEVER-FIRE is the introduction to models of the pyrogenic behaviour of humans, which is the timing of their activities and willingness or necessity to ignite or suppress fires. Such fire ignition or suppression is related to socioeconomic and demographic conditions in the geographical domain of the model application, with the aim of improving the representation of fire processes(33). Here, we add two main demographic controls on fire dynamics, namely population density (POP) that determines human potential ignitions, and urbanization. The second urbanization control is described by two further quantities: a ratio of rural to total population (RUR) and the distance from cities, *i.e.*, human settlements (DIS). These two variables reflect both the positive and negative influences of urbanization on area burned, due to creating increasing human ignitions in the WUI and enhanced fire suppression strategies, respectively (SI Appendix, Fig. S7). A constant present-day data-based mask for known cropland extent is applied to LPJ-SEVER. It is assumed that there are no fires over cropland, and therefore deforestation fires for agricultural expansion are not considered, which are typically considered in the estimate of the land-use flux, rather than fire flux, *i.e.*, the influences of present-day land use on fire and associated feedbacks are included in this study. Although land-use and land-cover change are not formally simulated, key aspects are implied via changes to fire activity in both urban and rural areas as wildland is urbanized. LPJ-SEVER simulates terrestrial biogeochemical process with fire disturbance and provides the land feedback of CO_2 to atmosphere based on changes to Net Biome Productivity (NBP). This flux is calculated as integrating gridbox mean values of net primary production minus heterotrophic respiration and fire carbon emissions.

Gridded climate and socioeconomic data compose external inputs for LPJ-SEVER(33). LPJ-SEVER is forced in total by gridded climate (temperature, minimum and maximum temperature, precipitation and convective precipitation, cloud cover, and wind speed), a land use ‘mask’, and socioeconomic data of POP, RUR, and DIS. Here, variable DIS is initially defined as the distance from the grid cell to the nearest grid cell with a population density exceeding 400 per km^{-2} (33), which is considered a threshold for an urban system(63, 64). A map of the spatial pattern of the present-day (the year 2010) cropland fraction is derived from the Land Use Harmonization dataset (LUH2)(65)

IMOGEN climate-fire-carbon cycle framework

To provide climate change drivers, LPJ-SEVER is coupled to the Integrated Model Of Global Effects of climatic aNomalies (IMOGEN)(66). IMOGEN generates smoothly changing climatic anomalies and by emulating 34 Earth System Models (ESMs) of the Coupled Model Intercomparison Project Phase 5 (CMIP5). These anomalies are added to a common base climatology, which is period 1901-1930 and from the CRU dataset(67). The anomalies of interannual variability for that period are also sampled randomly, and for future years these are added to the smoothly changing climatic projections. IMOGEN contains monthly geographical patterns of local meteorological changes, and the 34 CMIP5-based sets of these allow exploration of uncertainty from climate forcing(68). Specifically, IMOGEN employs climate 'pattern-scaling'(69) to calculate change, where regional and seasonal changes are assumed linear in global warming over land(66, 70), and with this providing a numerically efficient way to project change. An Energy Balance Model (EBM) calculates global warming amounts by changes in atmospheric GreenHouse Gases (GHGs), also fitted to the CMIP5 ensemble, and so enables the representation of the different climate sensitivities for ESMs. IMOGEN is operated 'online' with a closed carbon cycle and thus forced with anthropogenic CO_2 emissions. Annual CO_2 concentrations are updated at the end of each simulation year by annual CO_2 emissions due to fossil fuel burning, and changes in global land- and ocean-atmosphere carbon fluxes, derived from LPJ-SEVER and a simple global oceanic model, respectively(71). The extra radiative forcing change from non-CO_2 GHGs and aerosols is prescribed to the energy balance model(70), *i.e.,* aerosol effects from changes in fire regimes are not included. IMOGEN-LPJ-SEVER composed the coupled model framework aiming for assessing the interaction and feedback between atmosphere and land derived from changing fires. Non-CO_2 land-atmosphere emissions are not included in this study.

Scenarios

CO_2 emission scenarios. The IMOGEN-LPJ-SEVER coupled climate-fire-carbon cycle model was forced by prescribed fossil fuel CO_2 emissions. These were based on historical records over the period 1860-2005, followed by one of four future scenarios for period 2006-2100. The four emissions profiles were compatible with the Intergovernmental Panel on Climate Change Fifth Assessment Report (IPCC AR5) Representative Concentration Pathways (RCPs), *i.e.*, RCP2.6, RCP4.5, RCP6.0, and RCP8.5.

Socioeconomic scenarios. The initial base map of historical spatial gridded (urban) population density (POP) was for the period 1950-1959, and was derived from the United Nations Population Division (https://esa.un.org/unpd/wpp/Download/Standard/Population/). We used annual mean population growth rates from World Bank World Development Indicators (WDI). These values were historical annual average population growth rates, from which we calculated the gridded population density over the period 1960-2005 by multiplying them by the common base map numbers. Similarly, for the future, we extracted the annual average population growth rates from three Shared Socioeconomic Pathways (SSPs)(28), of SSP2, SSP3, and SSP5. These three scenarios gave the future gridded population density over the period 2006-2100. The criteria of selection for SSP socioeconomic scenarios had been extensively discussed in ref. (14). The SSPs could be broadly summarised as follows: SSP2 was a scenario with middle population density growth, urbanization, and economic growth, reflecting an intermediate pathway; SSP3 represented rapid population growth but slow urbanization and economic growth, leading to a high challenge of mitigation and adaptation; and SSP5 described a world with conventional economic growth and substantial fossil fuels consumption, leading to rapid urbanization but with slower population growth(14). In parallel, we derived the projections of the ratio of rural to total population (RUR) for the period 1950-2100 according to urban population density base map, and urbanization rate. The historical urbanization rate was derived from World Urbanization Prospects (WUP2009; https://sdi.eea.europa.eu/).

The average distance from a nearest city (DIS) was used as a proxy variable for (active and passive) fire suppression, determining fire duration, and as expected, it was strongly related to levels of urbanization (here mainly representing urban expansion). For example, an increasing urbanization reduced DIS, promoting fire suppression at the WUI due to safety reasons, resulting in a shorter fire duration and usually a smaller burned area. In general, global urban areas were growing on average twice as fast as urban populations(72) and this was in keeping with power scaling relationships in cities that had remained valid over many centuries(73). However, a parameter *coef*, defined as the ratio of urban area growth rate to urban population growth rate varied geographically. In particular, *coef* was country-dependent, relying on different strategies of regional socioeconomic development(74). This parameter allowed us to calculate the required urban area growth rate from the urban population growth rate. We assumed that the distance from a city changes at the same rate as the growth of urban areas. The base map of DIS, on a grid spacing of (3.75° × 2.5°) and used at the start of simulations, was interpolated from a dataset with (0.5° × 0.5°) spatial resolution in ref. (33). Based on the 'low projection' scenario (*i.e.*, assuming constant urban densities) of Tables 6.1 and 6.2 in ref. (74), we calculated the parameter *coef* in five regions. These corresponded to the aggregated five regions defined in SSPs (SI Appendix, Table S6), and thus we obtained the growth rate of DIS for the historical and future period, years 1950-2100. The socioeconomic data of the year 1950 was also used for the period 1860-1949 of the simulations. All the gridded datasets used in this study were prepared at a spatial resolution of 3.75° longitude × 2.5° latitude, in keeping with associated patterns of IMOGEN. Nearest neighbour interpolation method was used if needed.

Experimental design

Model initialization. The coupled IMOGEN-LPJ-SEVER model was started from 'bare ground' (*i.e.*, no plant biomass) and 'spun up' for 1001 model years until a good approximation to an equilibrium of carbon pools and vegetation cover was reached(71). Similar to the transient climate simulation, this spin-up was forced by a random sequence of years between 1901 and 1930, and from the CRU dataset. During this model initialization, there were no anthropogenic CO_2 emissions, no feedbacks from land and ocean to the atmosphere, and the socioeconomic data was fixed as that applicable to the year 1950. For the 'standard' and 'constant fire' experiments, fire disturbance was included in the spin-up, but was not present in the initialization used to start the 'without fire' experiments (See Table 1).

Offline simulations. For our historical offline simulations performed to verify model performance, LPJ-SEVER was run from a preindustrial equilibrium state and over the historical period 1950–2016. The model was driven using observed fields of monthly climatology CRU datasets and NCEP/NCAR Reanalysis datasets(75, 76), as well as observed annual global atmospheric CO_2 concentration(71). The input soil texture data was the same as ref. (58). No land or ocean carbon cycle feedbacks were included at this stage(71).

Model validation. Model validation contained two parts. The first part was verification of simulated global burned area and fire carbon emissions with SEVER-FIRE, and the second part was the comprehensive testing of the host land model, LPJ-DGVM. SEVER-FIRE had already been extensively validated in a previous study(33). Here, we added to such SEVER-FIRE testing by comparing its temporal and spatial projections (including their performance across different PFTs) against satellite-based global datasets of burned area and fire carbon emissions. This comparison used the model structure as driven 'offline' by the observed CRU and NCEP/NCAR climatologies(75, 76). We selected Global Fire Emissions Database version 4 product (GFED4)(77) , GFED4 that includes small fires (GFED4s)(1), and the version 5.0 of the Fire_CCI BA products (FireCCI50)(78) from the European Space Agency Climate Change Initiative as benchmarked burned area datasets. And GFED4s and Fire Energetics and Emissions Research version 1.0 (FEER1)(79) were used for fire carbon emission comparison. GFED4s fire emissions were calculated by GFED4s burned area, specified Combustion Completeness (CC), and vegetation biomass estimate from a biogeochemical model (CASA)(10, 61). FEER1 was developed using Fire Radiative Power (FRP) and constrained by satellite-based Aerosol Optical Depth (AOD). Rigorous benchmarking testing was also important to evaluate the performance of any underlying land model(80, 81). Therefore, we also performed a comprehensive validation of our dynamic global vegetation model, LPJ, and using the International Land Model Benchmarking (ILAMB) system. The ILAMB framework enabled the performing of tests for a wide range of land carbon and hydrology cycle variables and climate forcings, all against *in situ*, remote sensing, and reanalysis datasets(80). More details about the benchmarking test could be found in the SI Appendix, Fig. S4, Tables S2 and S5. Finally, an assessment of the simulated present-day global vegetation distribution was also provided.

Coupled climate-fire-carbon cycle simulations with changing fire, with constant fire, and without fire. First, we performed four 'standard' sets of coupled experiments (see Table 1), and dynamic fire disturbance was included. For these, the IMOGEN-LPJ-SEVER coupled model started from its preindustrial equilibrium at 1860 after 1001 years of model spin-up. Once the equilibrium state was reached, LPJ-SEVER was then run in transient mode forced by the IMOGEN framework. For each set of coupled experiments, 34 simulations were made, corresponding to each of the ESMs that IMOGEN emulates. The uncertainties from using different ESMs are referred to as 'climatic uncertainty'. The prescribed fossil fuel CO_2 emissions and external demographic and socioeconomic input (*i.e.*, via POP, RUR, and DIS variables) used historical levels for the period 1860-2005, then followed by one of four RCP CO_2 emission scenarios. For each of the four simulations, components of three Shared Socioeconomic Pathways (SSP) were also used and for the period 2006-2100. That was, each RCP scenario was initially aligned to a specific SSP combination (see Table 1). Inclusion of a 'constant fire' experiment has been used to investigate the role of changing fires on land carbon balance(11, 18). Here, in parallel to 'standard' experiments, we performed four further sets of 'constant fire' numerical experiments using IMOGEN-LPJ-SEVER coupled model under the identical experimental scenarios (see Table 1). Following the 1001-year model initialization in 'standard' experiment, using the same configurations to 'standard' spin-up, we performed 241 more years of 'spin-up extension' experiments to generate for each grid cell a fixed 241-year series of preindustrial burned area using recycling preindustrial climate and its variability. Then, we applied this 'constant fire' regime to the transient simulations over the period 1860-2100. Our 'constant fire' regime represented 'constant' burned area or burned fraction, but not constant fire carbon emission, as the latter was also dependent on fuel combusted which in turn varied with climate change and atmospheric CO_2 content (SI Appendix, Fig. S17). Comparison between 'standard transient fire' simulation with a world without fire has been widely used to investigate the role of fire on land carbon, water, or biome composition(3, 5, 37, 38). Therefore, in parallel to 'standard' experiments, we performed four final sets of 'without fire' experiments using IMOGEN-LPJ-SEVER coupled model under the identical experimental scenarios (see Table 1). All the configurations, and including initial atmospheric CO_2 concentration and climate state, in the 'without fire' simulations were identical to those used in the 'standard' simulations. The single difference is that the fire module was off during both the spin-up and the transient simulation over the modelled period of 1860-2100. Both land and ocean carbon cycle feedbacks were included in 'standard', 'constant fire', and 'without fire' simulations.

To estimate the uncertainties from demographic influences on fire dynamics, and their related impacts on the carbon balance and thus feedbacks to climate, we performed three additional ('standard', 'constant fire', and 'without fire') extra sets of simulations. These experiments were for four RCP scenarios, and each with 9 SSP combinations, giving 36 simulations. These calculations covered the range of possibilities in population growth and urbanization rates, and for three elected SSPs. These additional simulations (referred to as 'demographic uncertainty'; see SI Appendix, Table S1) were forced by one ESM (CESM1-BGC). This ESM had a roughly middle global land temperature change in the year 2100 relative to preindustrial, and when compared to the other ESMs emulated (SI Appendix, Fig. S18).

Analysis

The main metric for analysis was that of the difference between the coupled climate-fire-carbon cycle simulations with changing fire representation, versus those with a prescribed constant fire regime, and those without fires. The emphasis was placed on the differences that fire caused to components of the global carbon cycle, and in particular the net land carbon balance and resultant feedbacks to climate system via atmospheric CO_2 changes. We used 'climatic uncertainty' and 'demographic uncertainty' simulations to investigate the impact of uncertainties of climatic variation and human demography. A small technical point was that the effect of changing fires existed as an initial but small signal in climate (*e.g.*, temperature) during period 1860-1949 in 'standard' simulations. This omission was owing to the absence of the demographic and socioeconomic input for the fire model before year 1950. Pearson correlation analysis was used to test the temporal and spatial correlation between the 'offline' simulated and observed burned area and fire carbon emissions. Following ref. (29), we used a square root transformation on both the simulated and observed grid-cell-based burned area and fire carbon emissions due to the skewed distribution of burned area. This transformation removed skewness, as required for the Pearson correlation analysis. A Mann–Kendall test was used to test the significance of trends in burned area and fire carbon emissions.

The EBM part of IMOGEN calculated two large-scale temperatures, of spatial-mean annual temperature increase over land $\Delta T_{Land,yr}$ (°C) and spatial-mean annual increase for the ocean surface $\Delta T_{Ocean,yr}$(°C) (66, 69). It was the land temperature rise that multiplied the 'patterns' of climate change in the IMOGEN model framework. However, global temperature change was the main quantity to explore the global effects of carbon feedback to climate due to changing fires. Following ref. (66), global (spatial-) mean annual average temperature change, $\Delta T_{Global,yr}$ (°C) was computed as:

$$\Delta T_{Global,yr} = f \times \Delta T_{Ocean,yr} + (1 - f) \times \Delta T_{Land,yr}, \quad (1)$$

where yr was simulation year, $f \sim 0.71$ was the ESM-specific parameter of the global fraction of Earth covered by ocean.

Data Availability

All data used to evaluate the conclusions of the paper and generate the figures and tables are available at https://doi.org/10.6084/m9.figshare.12279404. The python codes to interpret data and prepare the figures are available on request from the corresponding author. We thank the Global Fire Emissions Database (GFED), European Space Agency Climate Change Initiative BA product (FireCCI), and Fire Energetics and Emissions Research (FEER), CMIP5 database, ILAMB, and other researchers who worked to provide the datasets for this study. Satellite-based GFED4s, GFED4 dataset are accessed from http://www.globalfiredata.org/index.html; FireCCI50 dataset was accessed from https://climate.esa.int/en/projects/fire/. FEER1 dataset is accessed from https://feer.gsfc.nasa.gov/data/emissions/. NCEP Reanalysis data provided by the NOAA/OAR/ESRL PSD, Boulder, Colorado, USA, from their Web site at https://www.esrl.noaa.gov/psd/. The IMOGEN model and the latest version is available from C.H. (contacted on chg@ceh.ac.uk).

Acknowledgements

The simulations were performed on the platform of University of Exeter, UK. We thank Felix Leung, Shushi Peng, Jun Yang, Staver lab members, and Wei Li who gave valuable comments about this work. We thank the editor and anonymous reviewers for their valuable comments, which have contributed to an improved paper. This work was supported by the National Key R&D Program of China (2019YFA0606604), the National Natural Science Foundation of China (31570475), Tsinghua University- Peter the Great St. Petersburg Polytechnic University Joint Scientific Research Fund (20193080033) (C.W. and S.V.), and China Scholarship Council (C.W.). SV acknowledges support of Russian State Assignment of the Federal Research Centre The Southern Scientific Centre of the Russian Academy of Sciences (SSC RAS) (122013100131-9) C.H. acknowledges the National Capability grant awarded to the UK Centre for Ecology and Hydrology by the Natural Environment Research Council. L.M.M. and S.S. are partly supported by the Newton Fund through the Met Office Climate Science for Service Partnership Brazil (CSSP Brazil), and Natural Environment Research Council (NERC) grants (NE/R001812/1 & NE/J010057/1). L.M.M. was also partly supported by the UK Natural Environment Research Council through The UK Earth System Modelling Project (UKESM, Grant No. NE/N017951/1). C.W. and A.C.S. were supported by a grant from the National

Science Foundation to A.C.S. (MSB #1802453). S.A. was supported by the NRF Earth Systems Grant 118604.

References

1. G. R. van der Werf *et al.*, Global fire emissions estimates during 1997–2016. *Earth Syst. Sci. Data* **9**, 697-720 (2017).

2. A. F. A. Pellegrini *et al.*, Fire frequency drives decadal changes in soil carbon and nitrogen and ecosystem productivity. *Nature* **553**, 194-198 (2018).

3. G. Lasslop *et al.*, Global ecosystems and fire: Multi-model assessment of fire-induced tree-cover and carbon storage reduction. *Glob. Chang. Biol.* **26**, 5027-5041 (2020).

4. D. S. Ward *et al.*, The changing radiative forcing of fires: global model estimates for past, present and future. *Atmos. Chem. Phys.* **12**, 10857-10886 (2012).

5. W. J. Bond, F. I. Woodward, G. F. Midgley, The global distribution of ecosystems in a world without fire. *New Phytol.* **165**, 525-537 (2005).

6. D. M. Bowman *et al.*, Fire in the Earth system. *Science* **324**, 481-484 (2009).

7. S. P. Harrison *et al.*, The biomass burning contribution to climate–carbon-cycle feedback. *Earth Syst. Dynam.* **9**, 663-677 (2018).

8. J. R. Marlon *et al.*, Climate and human influences on global biomass burning over the past two millennia. *Nat. Geosci.* **1**, 697-702 (2008).

9. O. Pechony, D. T. Shindell, Driving forces of global wildfires over the past millennium and the forthcoming century. *Proc. Natl. Acad. Sci. U S A* **107**, 19167-19170 (2010).

10. V. K. Arora, J. R. Melton, Reduction in global area burned and wildfire emissions since 1930s enhances carbon uptake by land. *Nat. Commun.* **9**, 1326 (2018).

11. Y. Yin *et al.*, Fire decline in dry tropical ecosystems enhances decadal land carbon sink. *Nat. Commun.* **11**, 1900 (2020).

12. S. Piao *et al.*, Lower land-use emissions responsible for increased net land carbon sink during the slow warming period. *Nat. Geosci.* **11**, 739-743 (2018).

13. T. F. Keenan *et al.*, Recent pause in the growth rate of atmospheric CO2 due to enhanced terrestrial carbon uptake. *Nat. Commun.* **7**, 13428 (2016).

14. W. Knorr, A. Arneth, L. Jiang, Demographic controls of future global fire risk. *Nat. Clim. Chang.* **6**, 781-785 (2016).

15. J. T. Abatzoglou, A. P. Williams, Impact of anthropogenic climate change on wildfire across western US forests. *Proc Natl Acad Sci U S A* **113**, 11770-11775 (2016).

16. F. Li, S. Levis, D. S. Ward, Quantifying the role of fire in the Earth system - Part 1: Improved global fire modeling in the Community Earth System Model (CESM1). *Biogeosciences* **10**, 2293-2314 (2013).

17. K. Thonicke *et al.*, The influence of vegetation, fire spread and fire behaviour on biomass burning and trace gas emissions: results from a process-based model. *Biogeosciences* **7**, 1991-2011 (2010).

18. N. Andela *et al.*, A human-driven decline in global burned area. *Science* **356**, 1356-1362 (2017).

19. I. Bistinas, S. P. Harrison, I. C. Prentice, J. M. C. Pereira, Causal relationships versus emergent patterns in the global controls of fire frequency. *Biogeosciences* **11**, 5087-5101 (2014).

20. V. C. Radeloff *et al.*, Rapid growth of the US wildland-urban interface raises wildfire risk. *Proc Natl Acad Sci U S A* **115**, 3314-3319 (2018).

21. O. Price, R. Bradstock, Countervailing effects of urbanization and vegetation extent on fire frequency on the Wildland Urban Interface: Disentangling fuel and ignition effects. *Landscape Urban Plann.* **130**, 81-88 (2014).

22. T. Schoennagel, C. R. Nelson, D. M. Theobald, G. C. Carnwath, T. B. Chapman, Implementation of National Fire Plan treatments near the wildland-urban interface in the western United States. *Proc Natl Acad Sci U S A* **106**, 10706-10711 (2009).

23. S. Archibald, D. P. Roy, B. W. Van Wilgen, R. J. Scholes, What limits fire? An examination of drivers of burnt area in Southern Africa. *Glob. Chang. Biol.* **15**, 613-630 (2009).

24. S. Hantson *et al.*, The status and challenge of global fire modelling. *Biogeosciences* **13**, 3359-3375 (2016).

25. A. Arneth *et al.*, Terrestrial biogeochemical feedbacks in the climate system. *Nat. Geosci.* **3**, 525-532 (2010).

26. Y. Zou *et al.*, Using CESM-RESFire to understand climate–fire–ecosystem interactions and the implications for decadal climate variability. *Atmos. Chem. Phys.* **20**, 995-1020 (2020).

27. R. H. Moss *et al.*, The next generation of scenarios for climate change research and assessment. *Nature* **463**, 747-756 (2010).

28. K. Riahi *et al.*, The Shared Socioeconomic Pathways and their energy, land use, and greenhouse gas emissions implications: An overview. *Global Environ. Change. Hum. Policy Dimens.* **42**, 153-168 (2017).

29. L. Teckentrup *et al.*, Response of simulated burned area to historical changes in environmental and anthropogenic factors: a comparison of seven fire models. *Biogeosciences* **16**, 3883-3910 (2019).

30. F. Li *et al.*, Historical (1700–2012) global multi-model estimates of the fire emissions from the Fire Modeling Intercomparison Project (FireMIP). *Atmos. Chem. Phys.* **19**, 12545-12567 (2019).

31. R. Ramo *et al.*, African burned area and fire carbon emissions are strongly impacted by small fires undetected by coarse resolution satellite data. *Proc. Natl. Acad. Sci. U S A* **118**, e2011160118 (2021).

32. C. Wu *et al.*, Historical and future global burned area with changing climate and human demography. *One Earth* **4**, 517–530 (2021).

33. S. Venevsky, Y. Le Page, J. M. C. Pereira, C. Wu, Analysis fire patterns and drivers with a global SEVER-FIRE v1.0 model incorporated into dynamic global vegetation model and satellite and on-ground observations. *Geosci. Model Dev.* **12**, 89-110 (2019).

34. D. I. Kelley *et al.*, How contemporary bioclimatic and human controls change global fire regimes. *Nat. Clim. Chang.* **9**, 690-696 (2019).

35. N. Andela, G. R. van der Werf, Recent trends in African fires driven by cropland expansion and El Nino to La Nina transition. *Nat. Clim. Chang.* **4**, 791-795 (2014).

36. D. P. van Vuuren *et al.*, The representative concentration pathways: an overview. *Clim. Change* **109**, 5-31 (2011).

37. C. Yue, P. Ciais, P. Cadule, K. Thonicke, T. T. van Leeuwen, Modelling the role of fires in the terrestrial carbon balance by incorporating SPITFIRE into the global vegetation model ORCHIDEE - Part 2: Carbon emissions and the role of fires in the global carbon balance. *Geosci. Model Dev.* **8**, 1321-1338 (2015).

38. F. Li, B. Bond-Lamberty, S. Levis, Quantifying the role of fire in the Earth system – Part 2: Impact on the net carbon balance of global terrestrial ecosystems for the 20th century. *Biogeosciences* **11**, 1345-1360 (2014).

39. M. Flannigan, B. Stocks, M. Turetsky, M. Wotton, Impacts of climate change on fire activity and fire management in the circumboreal forest. *Glob. Chang. Biol.* **15**, 549-560 (2009).

40. P. Friedlingstein *et al.*, Global Carbon Budget 2020. *Earth Syst. Sci. Data* **12**, 3269-3340 (2020).

41. R. Seidl *et al.*, Forest disturbances under climate change. *Nat. Clim. Chang.* **7**, 395-402 (2017).

42. J. W. Veldman *et al.*, Tyranny of trees in grassy biomes. *Science* **347**, 484-485 (2015).

43. G. Durigan, Zero-fire: Not possible nor desirable in the Cerrado of Brazil. *Flora* **268**, 151612 (2020).

44. C. N. Berlinck, E. K. L. Batista, Good fire, bad fire: It depends on who burns. *Flora* **268**, 151610 (2020).

45. R. C. R. Abreu *et al.*, The biodiversity cost of carbon sequestration in tropical savanna. *Sci. Adv.* **3**, e1701284 (2017).

46. C. Wu *et al.*, Climate-induced fire regimes in the Russian biodiversity hotspots. *Glob. Ecol. Conserv.* **16**, e00495 (2018).

47. D. Lohmann, B. Tietjen, N. Blaum, D. F. Joubert, F. Jeltsch, Prescribed fire as a tool for managing shrub encroachment in semi-arid savanna rangelands. *J. Arid Environ.* **107**, 49-56 (2014).

48. S. G. Conard, T. Hartzell, M. W. Hilbruner, G. T. Zimmerman, Changing fuel management strategies - The challenge of meeting new information and analysis needs. *Int. J. Wildland Fire* **10**, 267-275 (2001).

49. D. M. J. S. Bowman, J. A. O'Brien, J. G. Goldammer, Pyrogeography and the Global Quest for Sustainable Fire Management. *Annu. Rev. Environ. Resour.* **38**, 57-80 (2013).

50. J. C. Aleman, O. Blarquez, C. A. Staver, Land-use change outweighs projected effects of changing rainfall on tree cover in sub-Saharan Africa. *Glob. Chang. Biol.* **22**, 3013-3025 (2016).

51. J. T. Randerson *et al.*, The impact of boreal forest fire on climate warming. *Science* **314**, 1130-1132 (2006).

52. C. Heinze *et al.*, ESD Reviews: Climate feedbacks in the Earth system and prospects for their evaluation. *Earth Syst. Dynam.* **10**, 379-452 (2019).

53. Y. Jiang *et al.*, Impacts of Wildfire Aerosols on Global Energy Budget and Climate: The Role of Climate Feedbacks. *J. Climate* **33**, 3351-3366 (2020).

54. G. Lasslop, A. I. Coppola, A. Voulgarakis, C. Yue, S. Veraverbeke, Influence of Fire on the Carbon Cycle and Climate. *Curr. Clim. Change Rep.* **5**, 112-123 (2019).

55. Z. Liu, A. P. Ballantyne, L. A. Cooper, Biophysical feedback of global forest fires on surface temperature. *Nat. Commun.* **10**, 214 (2019).

56. J. Ruffault, F. Mouillot, How a new fire-suppression policy can abruptly reshape the fire-weather relationship. *Ecosphere* **6**, art199 (2015).

57. T. Fréjaville, T. Curt, Seasonal changes in the human alteration of fire regimes beyond the climate forcing. *Environ. Res. Lett.* **12**, 035006 (2017).

58. S. Sitch *et al.*, Evaluation of ecosystem dynamics, plant geography and terrestrial carbon cycling in the LPJ dynamic global vegetation model. *Glob. Chang. Biol.* **9**, 161-185 (2003).

59. S. Venevsky, K. Thonicke, S. Sitch, W. Cramer, Simulating fire regimes in human-dominated ecosystems: Iberian Peninsula case study. *Glob. Chang. Biol.* **8**, 984-998 (2002).

60. G. R. van der Werf *et al.*, Interannual variability in global biomass burning emissions from 1997 to 2004. *Atmos. Chem. Phys.* **6**, 3423-3441 (2006).

61. G. R. van der Werf *et al.*, Global fire emissions and the contribution of deforestation, savanna, forest, agricultural, and peat fires (1997–2009). *Atmos. Chem. Phys.* **10**, 11707-11735 (2010).

62. C. V. J. Silva *et al.*, Estimating the multi-decadal carbon deficit of burned Amazonian forests. *Environ. Res. Lett.* **15**, 114023 (2020).

63. Y. Liu, S. R. Phinn, Modelling urban development with cellular automata incorporating fuzzy-set approaches. *Comput. Environ. Urban* **27**, 637-658 (2003).

64. H. Millward, Rural population change in Nova Scotia, 1991–2001: bivariate and multivariate analysis of key drivers. *Can. Geogr.* **49**, 180-197 (2005).

65. L. Ma *et al.*, Global rules for translating land-use change (LUH2) to land-cover change for CMIP6 using GLM2. *Geosci. Model Dev.* **13**, 3203-3220 (2020).

66. C. Huntingford *et al.*, IMOGEN: an intermediate complexity model to evaluate terrestrial impacts of a changing climate. *Geosci. Model Dev.* **3**, 679-687 (2010).

67. M. New, M. Hulme, P. Jones, Representing twentieth-century space-time climate variability. Part II: Development of 1901-96 monthly grids of terrestrial surface climate. *J. Climate* **13**, 2217-2238 (2000).

68. C. Huntingford *et al.*, Implications of improved representations of plant respiration in a changing climate. *Nat. Commun.* **8**, 1602 (2017).

69. C. Huntingford, P. M. Cox, An analogue model to derive additional climate change scenarios from existing GCM simulations. *Clim. Dyn.* **16**, 575-586 (2000).

70. C. Huntingford *et al.*, Simulated resilience of tropical rainforests to CO2-induced climate change. *Nat. Geosci.* **6**, 268-273 (2013).

71. S. Sitch *et al.*, Evaluation of the terrestrial carbon cycle, future plant geography and climate-carbon cycle feedbacks using five Dynamic Global Vegetation Models (DGVMs). *Glob. Chang. Biol.* **14**, 2015-2039 (2008).

72. K. C. Seto, B. Guneralp, L. R. Hutyra, Global forecasts of urban expansion to 2030 and direct impacts on biodiversity and carbon pools. *Proc Natl Acad Sci U S A* **109**, 16083-16088 (2012).

73. L. M. Bettencourt, J. Lobo, D. Helbing, C. Kuhnert, G. B. West, Growth, innovation, scaling, and the pace of life in cities. *Proc Natl Acad Sci U S A* **104**, 7301-7306 (2007).

74. S. Angel, J. Parent, D. L. Civco, A. Blei, D. Potere, The dimensions of global urban expansion: Estimates and projections for all countries, 2000-2050. *Prog. Plann.* **75**, 53-107 (2011).

75. I. Harris, P. D. Jones, T. J. Osborn, D. H. Lister, Updated high-resolution grids of monthly climatic observations – the CRU TS3.10 Dataset. *Int. J. Climatol.* **34**, 623-642 (2013).

76. E. Kalnay *et al.*, The NCEP/NCAR 40-Year Reanalysis Project. *Bull. Am. Meteorol. Soc.* **77**, 437-472 (1996).

77. L. Giglio *et al.*, Analysis of daily, monthly, and annual burned area using the fourth-generation global fire emissions database (GFED4). *J. Geophys. Res. Biogeosci.* **118**, 317-328 (2013).

78. E. Chuvieco *et al.*, Generation and analysis of a new global burned area product based on MODIS 250 m reflectance bands and thermal anomalies. *Earth Syst. Sci. Data* **10**, 2015-2031 (2018).

79. C. Ichoku, L. Ellison, Global top-down smoke-aerosol emissions estimation using satellite fire radiative power measurements. *Atmos. Chem. Phys.* **14**, 6643-6667 (2014).

80. N. Collier *et al.*, The International Land Model Benchmarking (ILAMB) System: Design, Theory, and Implementation. *J. Adv. Model Earth Sy.* **10**, 2731-2754 (2018).

81. D. I. Kelley *et al.*, A comprehensive benchmarking system for evaluating global vegetation models. *Biogeosciences* **10**, 3313-3340 (2013).

Figures legends

Figure 1. Present-day burned area and fire carbon emissions. (A) Global temporal burned area with fitted linear trends (dashed lines) over the period 1997-2013. The global burned area trend values (Trend), mean annual burned area (Mean), temporal correlation coefficients (r) and P-values (P-value) between the observed against simulated burned area are annotated. (B) Global temporal fire carbon emissions with fitted linear trends (dashed lines) over the period 1997-2013. The global fire carbon emissions trend values, mean annual fire carbon emissions, temporal correlation coefficients and P-values between the observed against simulated fire carbon emissions are annotated**.** The asterisks indicate whether the trend is statistically significant (Mann–Kendall test; ***$p<0.01$, ** $p<0.05$, * $p<0.1$). No marking implies no statistical significance. The FireCCI50 burned area dataset started in year 2002 while FEER1 fire carbon emissions dataset started in year 2003. SEVER-FIRE is run in ‘offline’ mode, driven by the observed climatologies.

Figure 2. Projected changes in fire carbon emissions and their effect on land carbon uptake. (A and B) Simulated evolution of global fire carbon (C) emissions difference presented as the 'standard' experiments minus the 'constant fire' experiments under four RCP scenarios (both panels) and over the period 1860-2100. Grey dashed lines are the zero line, and when curves are below this line, then fire carbon emissions tend to decrease relative to a constant preindustrial fire regime. (C and D) Simulated evolution of global land carbon uptake (NBP) difference presented as the 'standard' experiments minus the 'constant fire'. All experiments in these two panels correspond to the four main RCP scenarios, shown for the period 1860-2100. Grey dashed lines are the zero line, and when curves are below this line, then changing fires contribute to a relative land carbon source. Thick lines in panels (A) and (C) show the mean values simulated under the 'climatic uncertainty' simulation with 34 ESMs emulated. The spreads shown are for each RCP, and the shaded areas represent standard deviation across the runs. Thick lines in panels (B) and (D) represent the mean values simulated under the 'demographic uncertainty' simulation with CESM1-BGC across 9 SSPs combinations, but emulated one ESM CESM1-BGC, which has projected mid-range global land temperature increase in year 2100 (see Materials and Methods). The spreads shown are for each RCP, and the shaded areas represent standard deviation across the runs. Box plots to the right of panels A-D show the mean annual values over the period 2081-2100 and squares within the boxes represent mean values of ensemble members. The four RCP scenarios in (A–D) are described in Table 1 and SI Appendix, Table S1, respectively. Year 1950 is indicated and after that, transient human demographic variables are allowed (see Materials and Methods). (E and F) Spatial patterns of the mean annual NBP difference presented as the 'standard' experiments minus the 'constant fire' experiments under RCP2.6 (D) and 8.5 (E) scenarios over the period 2081-2100, respectively. Shown results are averaged grid-based NBP differences between 'climatic uncertainty' and 'demographic uncertainty' simulations. A positive NBP difference corresponds to where changes in fire carbon emissions enhanced the land carbon sink whereas a negative value indicates changes in fire carbon emissions contributed to land carbon source.

Figure 3. Changing fire effects on atmospheric CO_2 concentration and feedbacks to climate. (A–D) Simulated evolution of global atmospheric CO_2 concentration difference (A and B), and global mean temperature difference (C and D) presented as the 'standard' experiments minus the 'constant fire'. All experiments in these four panels correspond to the four main RCP scenarios, shown for the period 1860-2100. Thick lines in panels (A) and (C) show the mean values simulated under the 'climatic uncertainty' simulation with 34 ESMs emulated. The spreads shown are for each RCP, and the shaded areas represent standard deviation for the results across 34 ESMs. Thick lines in panels (B) and (D) represent the mean values simulated under the 'demographic uncertainty' simulation with one ESM, CESM1-BGC, but across 9 SSPs combinations. The spreads shown are for each RCP, and the shaded areas represent standard deviation for the results across 9 SSPs combinations. Box plots to the right of panels A-D show the mean annual values over the period 2081-2100 and squares within the boxes represent mean values of ensemble members. Grey dashed lines are the zero line, and when curves are below this line, then changing fires contribute a decrease to atmospheric CO_2 concentration in panels (A) and (B), and a relative cooling to global climate in panels (C) and (D), respectively. (E and F) Sensitivity of simulated global mean temperature difference to atmospheric CO_2 concentration difference induced by changes in fire carbon emissions. Shown are the values of the 'standard' experiments minus the 'constant fire' experiments under four RCP scenarios over the period 1860-2100. (E) Ensemble-mean annual values simulated under the 'climatic uncertainty' simulation with 34 ESMs (lines). (F) Ensemble-mean annual values simulated under the 'demographic uncertainty' simulation with the CESM1-BGC ESM and across 9 SSPs combinations (lines). The error bars represent the standard deviation across the 34 ESMs (E) or 9 SSP combinations ensemble members (F) in year 2100.

Figure 4. Uncertainties associated with demography-driven global changing fire carbon emissions and related temperature differences. Simulated evolution of global fire carbon emissions difference (A) and global mean temperature difference (B) presented as the 'standard' experiments minus the 'constant fire' under RCP2.6 over the period 1860-2100. Lines in panels (A) and (B) represent the values simulated under the 'demographic uncertainty' simulation with one ESM, CESM1-BGC, but across 9 SSPs combinations. 'pop' means population growth rate; 'urb' means urbanization rate; 'historical' means historical period; 'slow', 'mid', and 'rapid' reveal the general levels of population growth rate (pop) or urbanization rate (urb) over the future period. 'Case 1' represents the case using a specific RCP–SSP combination in Table 1. Grey dashed lines are the zero line, and when curves are below this line, then fire carbon emissions tend to decrease relative to a constant preindustrial fire regime in panel (A), and changing fires contribute a relative cooling to global climate in panel (B), respectively.

Figure 5. A comparison of the simulated mean annual global mean temperature difference presented as the 'standard' experiments minus either the 'constant fire' experiments or the 'without fire' experiments under four RCP scenarios over the period 2081-2100. Panel (A) shows the mean annual values over the period 2081-2100 simulated under the 'climatic uncertainty' simulations, emulating 34 ESMs. Panel (B) represents the mean annual values over the period 2081-2100 simulated under the 'demographic uncertainty' simulation with the single CESM1-BGC ESM, but considering 9 SSPs combinations. The boxplots represent interquartile range and median, whiskers extend to the 'minimum' and 'maximum' values of ensemble; squares within the boxes are the mean values of ensemble members. Grey dashed lines are the zero line, and when curves are below this line, then changing fires contribute a relative cooling to global climate.

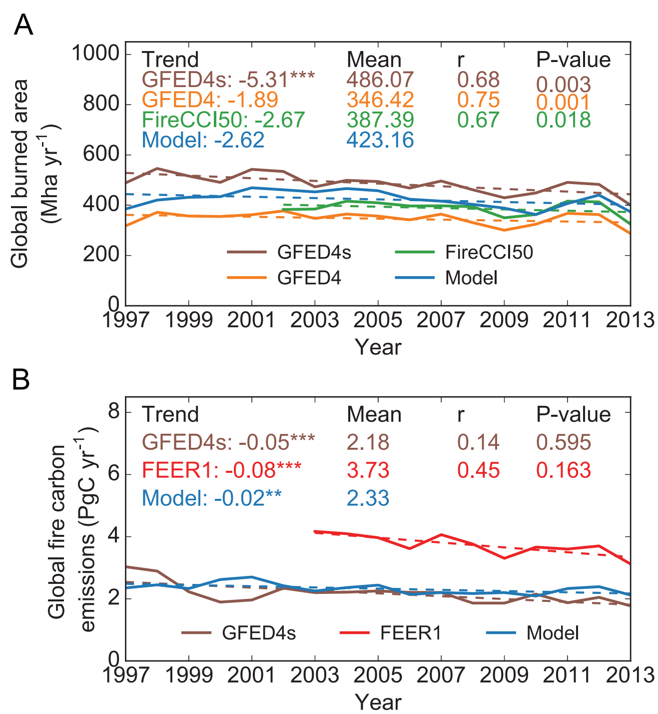
A
Trend
GFED4s: -5.31***
GFED4: -1.89
FireCCI50: -2.67
Model: -2.62
Mean
486.07
346.42
387.39
423.16
r
0.68
0.75
0.67
P-value
0.003
0.001
0.018
Global burned area (Mha yr^{-1})
1000
800
600
400
200
0
GFED4s
GFED4
FireCCI50
Model
1997
1999
2001
2003
2005
2007
2009
2011
2013
Year
B
Trend
GFED4s: -0.05***
FEER1: -0.08***
Model: -0.02**
Mean
2.18
3.73
2.33
r
0.14
0.45
P-value
0.595
0.163
Global fire carbon emissions (PgC yr^{-1})
8
6
4
2
0
GFED4s
FEER1
Model
1997
1999
2001
2003
2005
2007
2009
2011
2013
Year

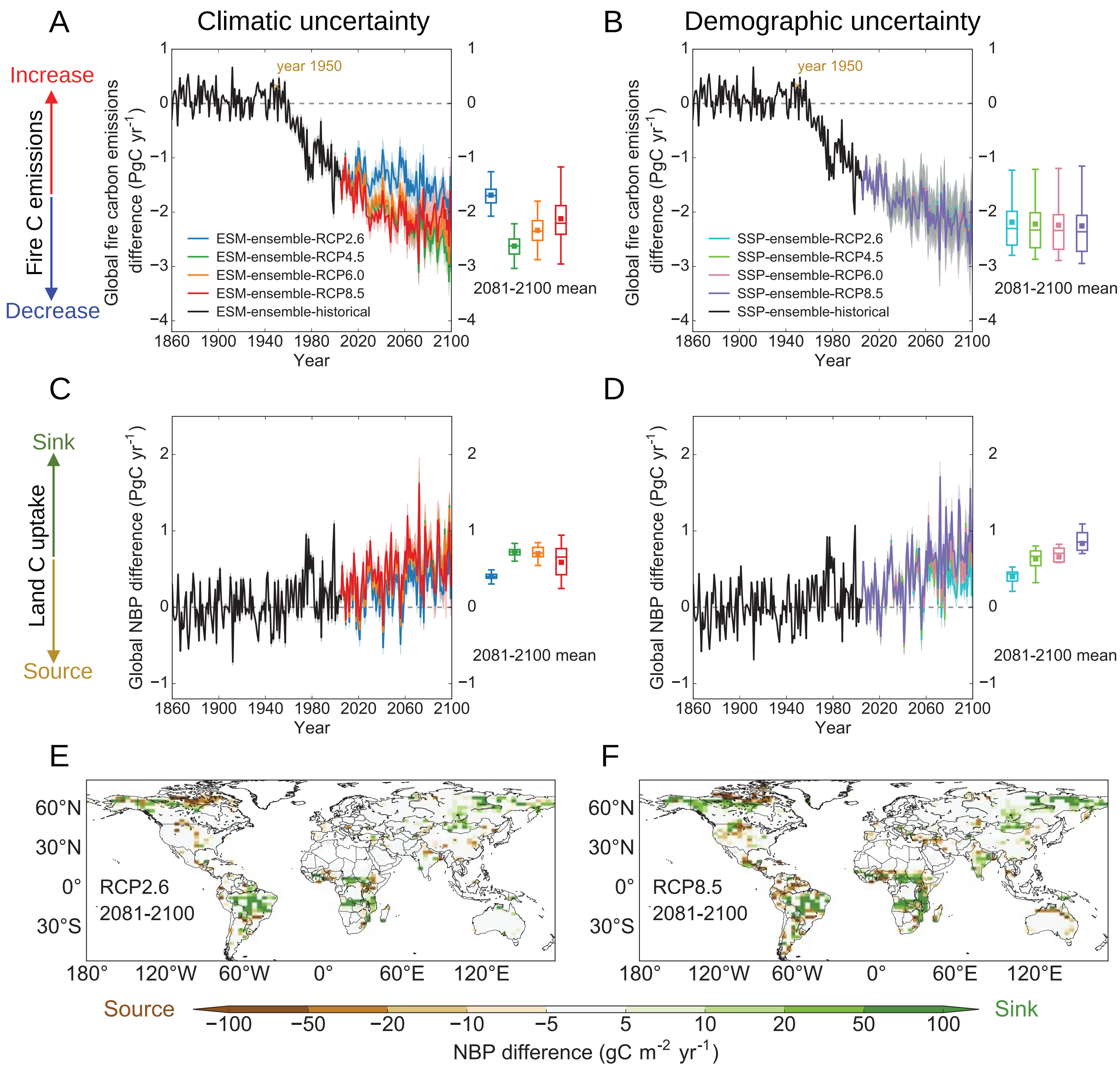

A
Climatic uncertainty
B
Demographic uncertainty
Increase
Fire C emissions
Decrease
Global fire carbon emissions difference (PgC yr-1)
year 1950
ESM-ensemble-RCP2.6
ESM-ensemble-RCP4.5
ESM-ensemble-RCP6.0
ESM-ensemble-RCP8.5
ESM-ensemble-historical
2081-2100 mean
SSP-ensemble-RCP2.6
SSP-ensemble-RCP4.5
SSP-ensemble-RCP6.0
SSP-ensemble-RCP8.5
SSP-ensemble-historical
Year
C
D
Sink
Land C uptake
Source
Global NBP difference (PgC yr-1)
E
F
RCP2.6
2081-2100
RCP8.5
2081-2100
60°N
30°N
0°
30°S
180°
120°W
60°W
0°
60°E
120°E
Source
Sink
−100
−50
−20
−10
−5
5
10
20
50
100
NBP difference (gC m-2 yr-1)

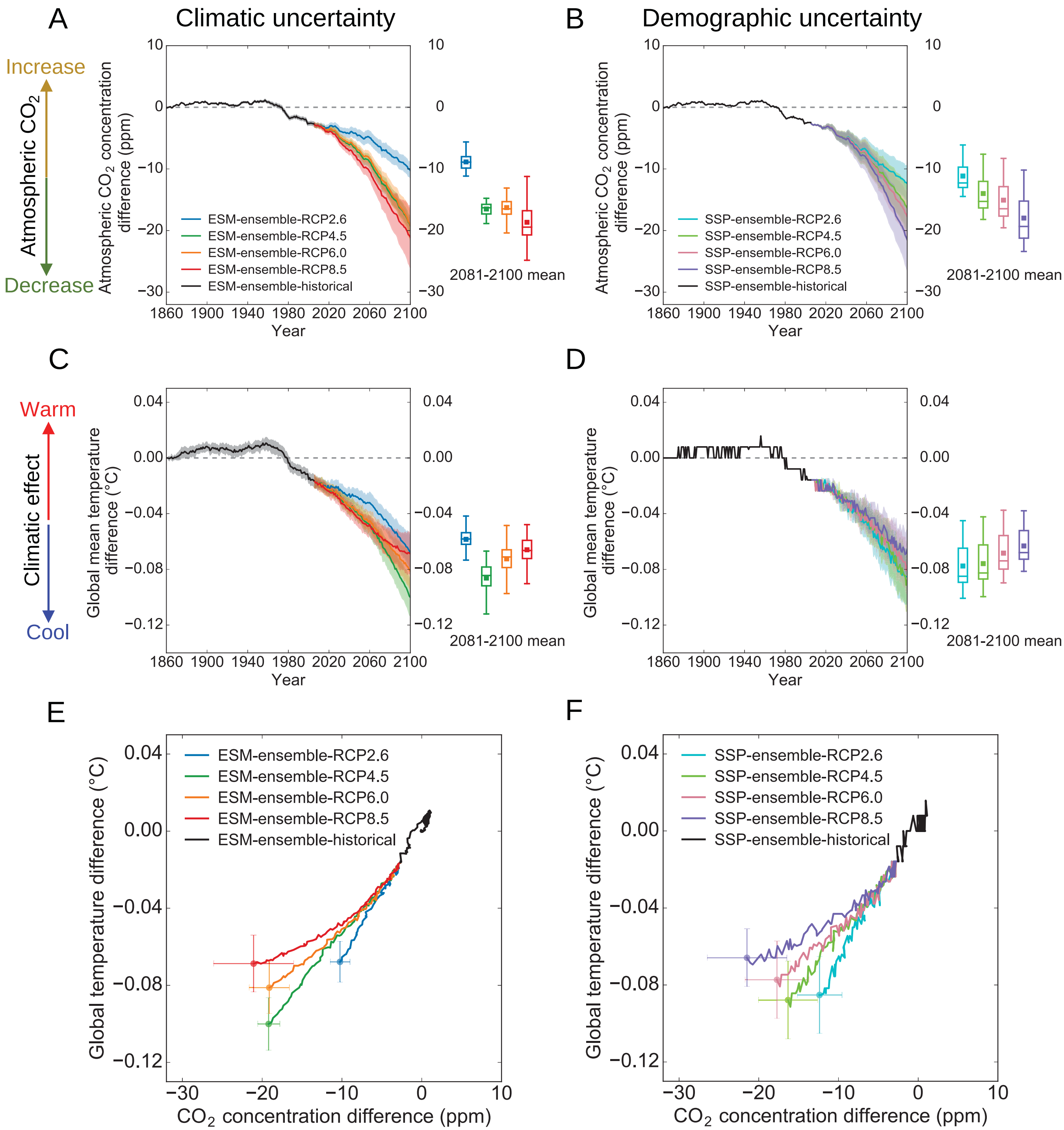

A
Climatic uncertainty
B
Demographic uncertainty
Increase
Atmospheric CO2
Decrease
Atmospheric CO2 concentration difference (ppm)
ESM-ensemble-RCP2.6
ESM-ensemble-RCP4.5
ESM-ensemble-RCP6.0
ESM-ensemble-RCP8.5
ESM-ensemble-historical
SSP-ensemble-RCP2.6
SSP-ensemble-RCP4.5
SSP-ensemble-RCP6.0
SSP-ensemble-RCP8.5
SSP-ensemble-historical
2081-2100 mean
Year
C
D
Warm
Climatic effect
Cool
Global mean temperature difference (°C)
E
F
Global temperature difference (°C)
CO2 concentration difference (ppm)

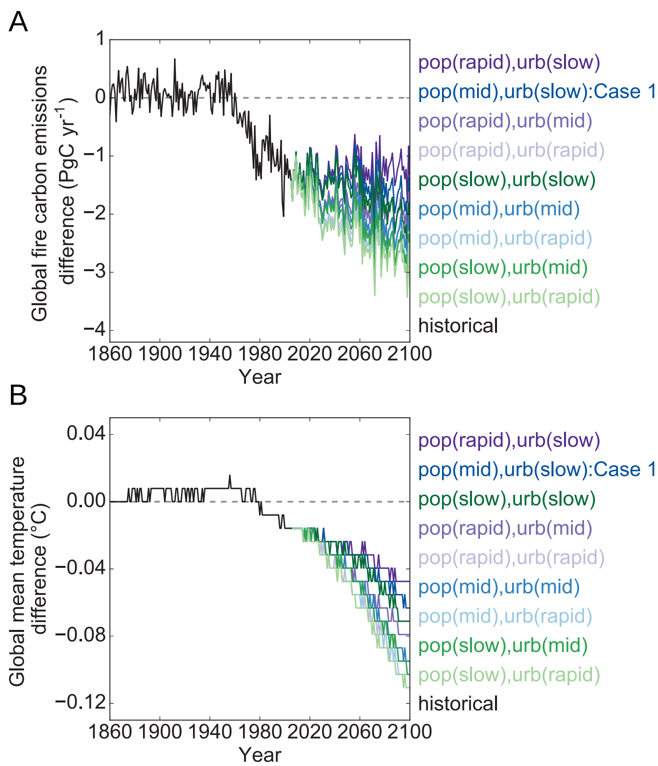

A
Global fire carbon emissions difference (PgC yr^{-1})
1
0
−1
−2
−3
−4
1860 1900 1940 1980 2020 2060 2100
Year
pop(rapid),urb(slow)
pop(mid),urb(slow):Case 1
pop(rapid),urb(mid)
pop(rapid),urb(rapid)
pop(slow),urb(slow)
pop(mid),urb(mid)
pop(mid),urb(rapid)
pop(slow),urb(mid)
pop(slow),urb(rapid)
historical
B
Global mean temperature difference (°C)
0.04
0.00
−0.04
−0.08
−0.12
1860 1900 1940 1980 2020 2060 2100
Year
pop(rapid),urb(slow)
pop(mid),urb(slow):Case 1
pop(slow),urb(slow)
pop(rapid),urb(mid)
pop(rapid),urb(rapid)
pop(mid),urb(mid)
pop(mid),urb(rapid)
pop(slow),urb(mid)
pop(slow),urb(rapid)
historical

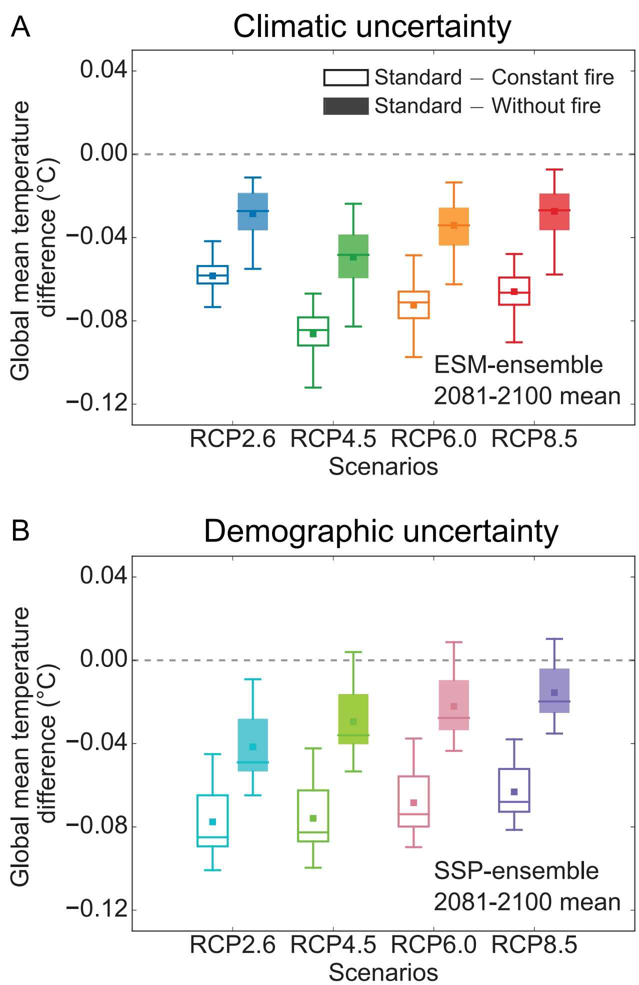
A
Climatic uncertainty
Standard – Constant fire
Standard – Without fire
Global mean temperature difference (°C)
0.04
0.00
−0.04
−0.08
−0.12
ESM-ensemble
2081-2100 mean
RCP2.6 RCP4.5 RCP6.0 RCP8.5
Scenarios
B
Demographic uncertainty
Global mean temperature difference (°C)
0.04
0.00
−0.04
−0.08
−0.12
SSP-ensemble
2081-2100 mean
RCP2.6 RCP4.5 RCP6.0 RCP8.5
Scenarios

Table 1. Experimental design in 'standard', 'constant fire', and 'without fire' simulations. Overview of the CO_2 emission and socioeconomic scenarios used in the 'standard', 'constant fire', and 'without fire' experiments.

	Cases	Spin-up includes fire	CO_2 emission scenarios	Socioeconomic scenarios		
				POP	Urbanization	
					RUR	DIS
'Standard' / 'Constant fire' experiments	1	yes	RCP2.6	SSP2(middle*)	SSP3(slow)	SSP3(slow)
	2	yes	RCP4.5	SSP5(slow*)	SSP2(middle)	SSP2(middle)
	3	yes	RCP6.0	SSP2(middle)	SSP2(middle)	SSP2(middle)
	4	yes	RCP8.5	SSP3(rapid*)	SSP5(rapid)	SSP5(rapid)
'Without fire' experiments	1	no	RCP2.6	SSP2(middle)	SSP3(slow)	SSP3(slow)
	2	no	RCP4.5	SSP5(slow)	SSP2(middle)	SSP2(middle)
	3	no	RCP6.0	SSP2(middle)	SSP2(middle)	SSP2(middle)
	4	no	RCP8.5	SSP3(rapid)	SSP5(rapid)	SSP5(rapid)

*'Slow', 'middle', and 'rapid' under 'population density (POP)' represent the general rates of population growth (pop), while in 'ratio of rural to total population (RUR)' and 'average distance from the nearest city (DIS)', they are urbanization rate (urb) (Materials and Methods). Four RCP CO_2 emission scenarios and three SSP socioeconomic scenarios are selected.